A "sliding box" automatic relocation method based on Geometric-mean reverse-time migration

Tong Bai[1], Zhendong Zhang[1], Malcolm C. A. White[1], Hongrui Qiu[1], Paul Williamson[2], and Nori Nakata[1,3]
1. Massachusetts Institute of Technology 2. TotalEnergies 3. Lawrence Berkeley National Laboratory

SUMMARY

Regional seismic networks typically monitor and locate seismic sources using only kinematic (i.e., traveltime) observations. We propose an automated "sliding box" procedure to improve source locations by leveraging dynamic (e.g., full waveform) information via Geometric-mean Reverse-Time Migration (GmRTM). We demonstrate the proposed method's efficacy by selecting and relocating some of the cataloged tectonic earthquakes recorded by a network of ~250 three-component seismic sensors deployed across 8,000 km^2 of mountainous terrain in Central Asia. Each event is recorded with sufficient signal-to-noise ratio (≥ 4) by at least 8 sensors inside a 20 km×20 km box centered on the cataloged location. For each event, we extract a local 3-D velocity model, multiply the waveform data by their corresponding STA/LTA ratios to suppress coda waves and other coherent noise, and apply GmRTM to reconstruct high-resolution source images. The automatic procedure reasonably relocates 280 earthquakes.

INTRODUCTION

Accurate earthquake locations are essential for many seismological studies, such as focal mechanism estimation, fault structure characterization, and geo-hazard monitoring. Compared with the conventional traveltime-based methods, the waveform-based method requires no phase picking. It is therefore particularly advantageous when working with low SNR data or data recording interfering wavefields from multiple events. Time-reversal imaging (TRI), one typical waveform-based method, has recently been applied successfully in both acoustic (Fink and Prada, 2001; Gajewski and Tessmer, 2005) and elastic media (Larmat et al., 2009; Artman et al., 2010; Saenger, 2011; Yang and Zhu, 2019), thanks to the increasing computational power.

However, the excitation time estimation required by TRI can be tedious and uncertain, and the image quality deteriorates with insufficient receiver sampling. To mitigate these problems, Nakata and Beroza (2015) and Sun et al. (2015) proposed the Geometric-mean reverse-time migration (GmRTM) method, which replaces the wavefield summation in TRI with cross-correlations. GmRTM has been successfully applied for imaging earthquake rupture (Yang et al., 2020) and microseismic events (Zhu et al., 2019; Wu et al., 2022). Bai et al. (2022b) comprehensively studied different receiver grouping strategies to balance image resolution and computational efficiency. For elastic media, GmRTM (Bai et al., 2022a) is further advantageous for image interpretation, in which the source location is often associated with zero-crossings in images produced by TRI.

It is often computationally challenging to apply waveform-based methods on a large study area for high-resolution source location. Furthermore, the image resolution obtained by TRI is restricted by inter-station distances, which often need to be large to cover the entire study area. Here, we propose an automated processing and relocation procedure: Instead of using the entire sensor array to image each earthquake, we implement a "sliding-box" strategy that only includes data recorded within a threshold distance from the catalog location. Limiting the data in this way ensures high signal-noise ratio and reduces model size (and thus computational expense). We also screen data based on data quality and the number of available receivers. Other key techniques that we apply include (a) STA/LTA filtering to suppress coda waves and (b) elastic GmRTM for superior image resolution. We demonstrate the approach using a land data set from Central Asia, which we describe below.

STUDY SITE

The study site is located in a mountainous area in Central Asia covering roughly 8,000 km^2. Data acquisition consists of two phases, each lasting about three months. During each phase, about 240 three-component (3C) stations (empty and filled triangles in Figure 1a for each phase) are deployed with an average inter-station distance of about 5 km. During the entire recording time, about 2,600 earthquakes, with magnitude between 0.5 and 2.5, are detected and located by a service company using a traveltime-based method. In addition, the regional 3-D V_P and V_S models are estimated using local earthquake traveltime tomography, which we use in this study for source relocation.

METHODOLOGY

Sliding study area selection

With the large (approximately 100 km × 80 km) and irregular array, we adopt a "sliding-box" strategy to reduce the size of our model domain for computational efficiency of our waveform-based method. Specifically, for each catalog event, we choose a 20 km × 20 km box (Figures 1) with its center at the catalog location to ensure an ideal recording geometry. Inside this box, we count the number of stations ($nrec$) with high signal-noise ratio data (see next subsection), and only image the events that contain at least 8 (i.e., $nrec \geq 8$). In the vertical direction, we reject cataloged events with depths of more than 12 km because wide-offset data are needed to accurately constrain the source depth in these cases. Our model size is 20 km × 20 km × 14 km, and the total number of target events we choose to relocate is 280.

Data preprocessing

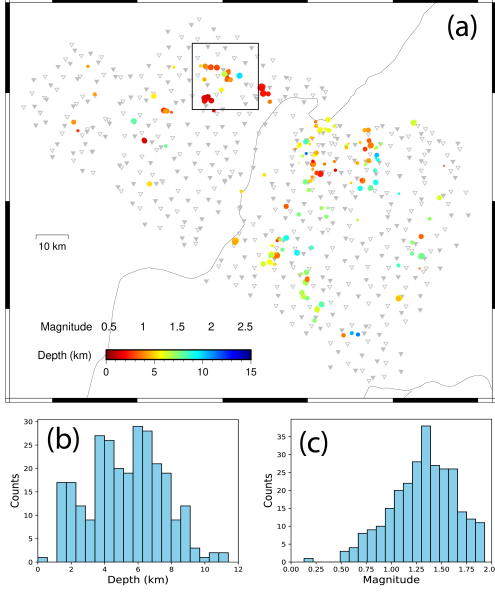We extract 20 s windows of 3C data for each event based on

Figure 1: (a) Acquisition map showing two-phase stations (inverse triangles) and selected 280 events (dots), whose colors and sizes reflect corresponding event depths and magnitudes. The black boxes mark the horizontal range of computational domain for the example event imaged in Figure 4. The histograms of (b) depth and (c) magnitude distributions.

the arrival times provided by the service company. We then remove the mean and trend of the data, before bandpass filtering it between 1 Hz and 5 Hz. Strong, coherent noise (primarily from coda waves) contaminates the preprocessed data and compromises imaging results. We overcome this challenge and improve our imaging results by adopting a characteristic function ($\sqrt{Z^2 + E^2 + N^2}$) that leverages all three data components to calculate the corresponding STA/LTA ratios. This procedure is frequently used to detect events, but we use the STA/LTA ratios here as an additional, multiplicative filter on the preprocessed data, which helps suppress the coda waves (Figure 2). Compared with hard-threshold selection methods that determine a window to isolate designated waves, our soft-threshold selection algorithm (by multiplying STA/LTA ratios) requires no manual setting of window sizes and threshold values and is also less sensitive to picking errors.

Elastic geometric-mean reverse-time migration
Like elastic TRI, the procedure of elastic GmRTM can be summarized in three steps: (1) back-injection of the time-reversed data (e.g., displacement, particle velocity), (2) wave-mode decomposition, and (3) application of imaging condition.

Bai et al. (2021) propose and implement a 2-D elastic GmRTM method using a PS source imaging condition:

$$I^{PS}_{G,2D}(\mathbf{x}) = \int_t \prod_{i=1}^{N} \Theta_i(\mathbf{x},t)\Phi_i(\mathbf{x},t), \qquad (1)$$

where Θ and Φ represent the decoupled scalar P- and SV-wavefields after Helmholtz decomposition, and the subscript
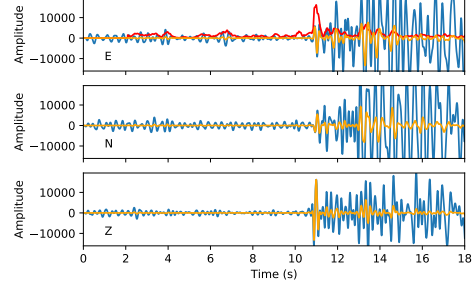

Figure 2: Sample three-component data at one station which records the event at the center of the box in Figure 1. Blue: the bandpass (1-5 Hz) filtered data. Red: the corresponding STA/LTA ratio. Orange: data in blue scaled by the STA/LTA ratio, which is used for source imaging.

i represents the ith receiver. In 3-D applications, vector P- and S-wavefields can be obtained (Zhu, 2017; Yang et al., 2018) and the PS-imaging condition becomes

$$I^{PS}_{G,3D}(\mathbf{x}) = \int_t \prod_{i=1}^{N} \vec{\Theta}_i(\mathbf{x},t) \cdot \vec{\Phi}_i(\mathbf{x},t). \qquad (2)$$

Finally, the grid point with the largest image intensity from $I^{PS}_{G,3D}(\mathbf{x})$ will be taken as the potential source location.

The entire workflow (Figure 3) can be summarized as: (1) local acquisition geometry conversion and local 3-D velocity models extraction; (2) data preprocessing (detrending, bandpass filtering, and STA/LTA filtering); (3) screening based on the number of eligible stations; (4) elastic source imaging via GmRTM; (5) maximum grid point picking. Steps (1)-(5) are repeated for all the catalog events. Finally, we convert all coordinates back to the absolute, global frame to obtain the relocated source distribution in local and global coordinates.

RESULTS

We scan the catalog (∼2,600 earthquakes during the total recording time of ∼6 months) and select 280 events for relocation based on the criterion discussed above. Figure 4 shows the GmRTM source image for one event, which is at the center of box a in Figure 1 and is displaced by about 1.1 km from the catalog location. The imaged source locations of all selected events are saved and can be shown in the relative coordinate system (blue dots in Figure 5), where all the catalog locations (red dots) are fixed at the center, or at the horizontal coordinate of (10 km, 10 km). The horizontal and total shifts from the catalog locations are also summarized as histograms as in Figure 6, which are mostly within 2 km and 5 km, respectively. The relocated source distribution in the relative coordinate system (Figure 5) and the histogram of shifts (Figure 6) provide qualitative and quantitative visualization of the location updates. Considering the average inter-station distance of about 5 km, we believe the relocation results are not significantly different from the catalog, which is based on a traveltime-based method using the entire receiver array.
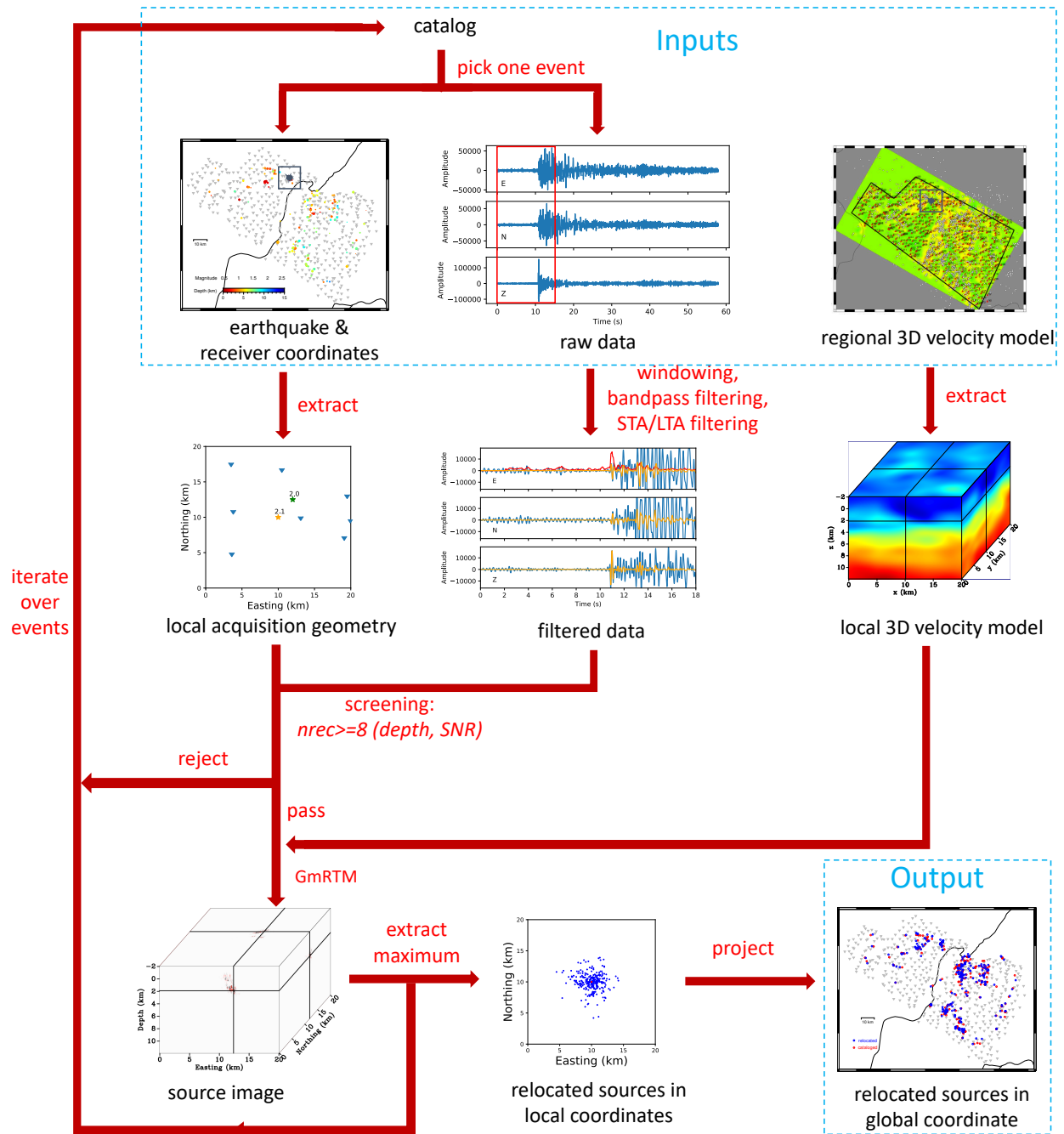
"Sliding-box" Automatic Relocation Method

Figure 3: The workflow of the proposed automatic processing and imaging procedure.

Finally, the relocated sources can be mapped back into the original absolute/global coordinate system (Figure 7). Again, the relocated results (blue dots) are not far away from the catalog results (red dots), and in fact, the relocated sources are overall more clustered, especially in tectonically active regions. Further validation and interpretation of the relocation results are the subject of ongoing work.
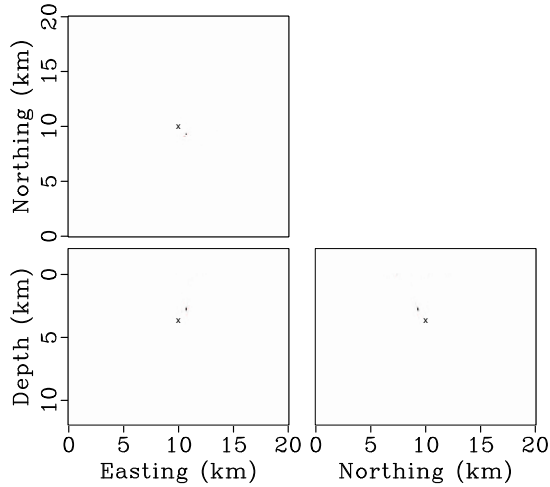
Figure 4: GmRTM image for the source in Figure 1a. The point with maximum intensity is at (x,y,z)=(10.7 km, 9.3 km, 2.9 km), and is about 1.1 km away from the catalog source location (marked by the cross), which is at (10 km, 10 km, 3.4 km).
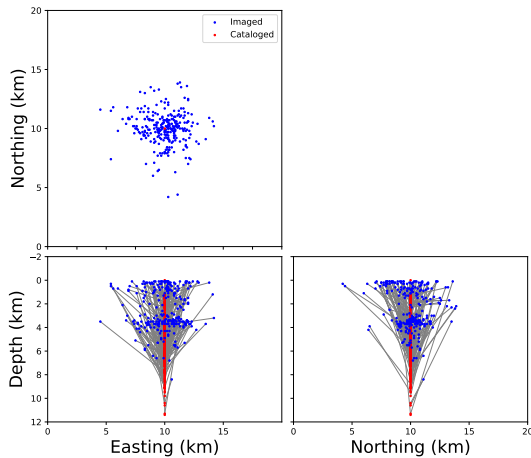

Figure 5: The cataloged (red) and relocated (blue) source distributions of the selected 280 events in the relative coordinate system.

CONCLUSIONS

We introduced an automated processing and relocation procedure based on Geometric-mean Reverse-Time Migration (Gm-RTM). It enables high-resolution microseismic/earthquake re-
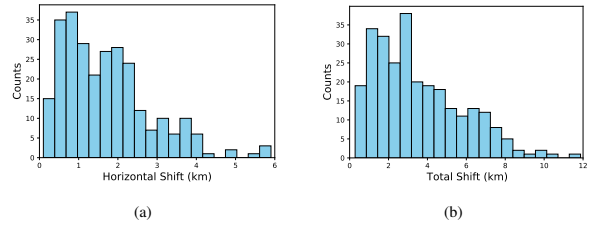

Figure 6: Histograms of the (a) horizontal and (b) total shifts between the cataloged and relocated sources.
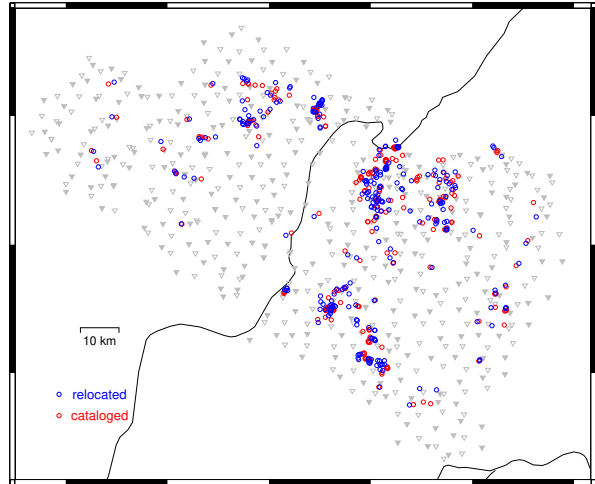

Figure 7: The cataloged (red) and relocated (blue) source distribution in the entire survey area.

location in large study areas, where traditional traveltime-based methods are often applied. The key steps include: (1) catalog-based "sliding" model space selection; (2) STA/LTA filtering for coda suppression; (3) strict screening criteria based on the data quality and receiver count; and (4) elastic GmRTM for high-resolution source imaging with sparse receivers.

We demonstrated the proposed procedure with a land data set from Central Asia, and relocated 280 earthquakes. Their horizontal and total shifts from the corresponding catalog locations are overall within 2 km and 5 km, respectively. Comprehensive validation and interpretation of the relocation results as well as sensitivity analysis of relocation accuracy and uncertainty covering key factors (e.g., maximum azimuthal gap, source-receiver distance, data SNR, event depth etc) is ongoing work and will be published later.

ACKNOWLEDGMENTS

REFERENCES

Artman, B., I. Podladtchikov, and B. Witten, 2010, Source location using time-reverse imaging: Geophysical Prospecting, **58**, 861–873.

Bai, T., B. Lyu, F. Gao, P. Williamson, and N. Nakata, 2021, Geometric-mean reverse-time migration for elastic media: Presented at the First International Meeting for Applied Geoscience & Energy, Society of Exploration Geophysicists.

Bai, T., B. Lyu, F. Li, P. Williamson, and N. Nakata, 2022a, Geometric-mean Reverse-Time Migration for elastic media: Geophysics, **Under revision**.

Bai, T., B. Lyu, P. Williamson, and N. Nakata, 2022b, Receiver grouping strategies for hybrid geometric-mean reverse time migration: Geophysics, **87**, KS45–KS55.

Fink, M., and C. Prada, 2001, Acoustic time-reversal mirrors: Inverse problems, **17**, R1.

Gajewski, D., and E. Tessmer, 2005, Reverse modelling for seismic event characterization: Geophysical Journal International, **163**, 276–284.

Larmat, C., R. Guyer, and P. Johnson, 2009, Tremor source location using time reversal: Selecting the appropriate imaging field: Geophysical Research Letters, **36**.

Nakata, N., and G. C. Beroza, 2015, Reverse-time migration for microseismic sources using the geometric mean as an imaging condition, *in* SEG Technical Program Expanded Abstracts 2015: Society of Exploration Geophysicists, 2451–2455.

Saenger, E. H., 2011, Time reverse characterization of sources in heterogeneous media: NDT & E International, **44**, 751–759.

Sun, J., T. Zhu, S. Fomel, and W.-Z. Song, 2015, Investigating the possibility of locating microseismic sources using distributed sensor networks, *in* SEG Technical Program Expanded Abstracts 2015: Society of Exploration Geophysicists, 2485–2490.

Wu, S., Y. Wang, F. Xie, and X. Chang, 2022, Crosscorrelation migration of microseismic source locations with hybrid imaging condition: Geophysics, **87**, KS17–KS31.

Yang, J., and H. Zhu, 2019, Locating and monitoring microseismicity, hydraulic fracture and earthquake rupture using elastic time-reversal imaging: Geophysical Journal International, **216**, 726–744.

Yang, J., H. Zhu, and D. Lumley, 2020, Time-lapse imaging of coseismic ruptures for the 2019 ridgecrest earthquakes using multiazimuth backprojection with regional seismic data and a 3-d crustal velocity model: Geophysical Research Letters, **47**, e2020GL087181.

Yang, J., H. Zhu, W. Wang, Y. Zhao, and H. Zhang, 2018, Isotropic elastic reverse time migration using the phase- and amplitude-corrected vector p-and s-wavefields: Geophysics, **83**, S489–S503.

Zhu, H., 2017, Elastic wavefield separation based on the helmholtz decomposition: Geophysics, **82**, S173–S183.

Zhu, T., J. Sun, D. Gei, J. M. Carcione, P. Cance, and C. Huang, 2019, Hybrid multiplicative time-reversal imaging reveals the evolution of microseismic events: Theory and field-data tests: Geophysics, **84**, KS71–KS83.